Enhancing the Information Capacity With Modulated Orbital Angular Momentum Holography

Feili Wang, Xiangchao Zhang ⓘ, *Member, IEEE*, He Yuan, Rui Xiong, and Xiangqian Jiang ⓘ

Abstract—The orbital angular momentum (OAM) holography has been developed and experimentally demonstrated the capability of holographic multiplexation and high-security encryption. However, the helical phase of an OAM mode can only be encoded into one hologram associated with a target image, and this severely limits the information capacity in practical applications. The modulated orbital angular momentum (MOAM) holography is proposed by imposing multiple modulation phase modes onto one OAM mode. Three essential properties, including the MOAM-preservation, MOAM-selectivity and MOAM-multiplexation are investigated. This method can significantly enhance the holographic information capacity and it has broad prospects for optical encryption and beam manipulations.

Index Terms—Modulated orbital angular momentum holography, holographic multiplexation, high-security encryption.

I. Introduction

ANGULAR momentum is an essential physical dimension of light beams besides the amplitude, phase, wavelength and polarization both in classical and quantum mechanics. A light beam can carry both spin angular momentum and orbital angular momentum (OAM), where the spin angular momentum is associated with the polarization state and the OAM is linked with the helical structure. The OAM introduced by Allen in 1992 [1] is represented by a helical wavefront of light $\exp(jl\varphi)$, where l and φ denote the helical mode index and the azimuthal angle, respectively, and j is the imaginary unit. At the center of an OAM-carrying beam, the intensity is zero and the phase is undetermined [2]. In recent years, OAM has been extensively investigated due to its interesting properties and widely applied in optical tweezers [3], [4], optical communications [5]–[7], meta-surfaces [8], and other fields.

In addition, the OAM can also be used to achieve high-security encryption. Recently, the OAM holography [8]–[10] was achieved for the reconstruction of multiple OAM-carrying images, without a theoretical limit of the helical phase index. An ordinary digital hologram is sampled first in its spatial frequency domain, where the sampling period is determined by the spatial-frequency bandwidth of the incident OAM beam, which obeys a doughnut-shaped intensity distribution. In order to maintain the OAM selectivity, a helical phase mode should be encoded onto the hologram. An OAM hologram can henceforth be generated for high-security optical encryption. However, in the existing methods [8], [9], a helical phase mode can only be encoded onto one hologram, implying that a helical phase index is only associated with one target image. In addition, the image resolution is restricted by the associated OAM modes.

A vortex beam with a phase map $\exp(jl\varphi)$ in the azimuthal direction carries OAMs [11]. In addition to the canonical vortex, the non-canonical vortex can also carry variable OAMs, such as non-symmetric vortex beams [12], [13], helico-conical beams [14], [15], fractional vortex beams [16], [17], Airy vortex beams [18]–[20], Pearcey vortex beams [21], [22] and so on, which have diverse propagation behaviors. The optics vortices can also be modulated [23]–[27]. For example, when the helical phase of an optics vortex is modulated by a cosine function, the beam will gradually split into several main lobes during propagation. The number, locations and rotation of the main lobes can be flexibly controlled by adjusting the modulation factors [24]. Fortunately, such an interesting property of the modulated orbital angular momentum (MOAM) provides additional degrees of freedom for beam manipulations and gives rise to improving the performance of the OAM holography.

As a consequence, we demonstrate the MOAM holography by imposing modulating phases onto an OAM mode. Then by multiplexing the OAM beam with multiple helical modes, a resolution enhancement can be achieved in the reconstructed holographic images. The rest of the paper is organized as follows. The principle of the MOAM holography is introduced in Section II. The properties and implementation of the MOAM holography are presented in Section III, and the paper is summarized in Section IV.

II. Principle of MOAM Holography

In the holographic imaging, the electric fields on the hologram plane $H(k_x, k_y)$ and the image plane $E(x, y)$ form a Fourier pair, where x and y are the transversal coordinates on the image plane, and k_x and k_y are the transversal coordinates on the hologram plane. We introduce a modulated orbital angular momentum
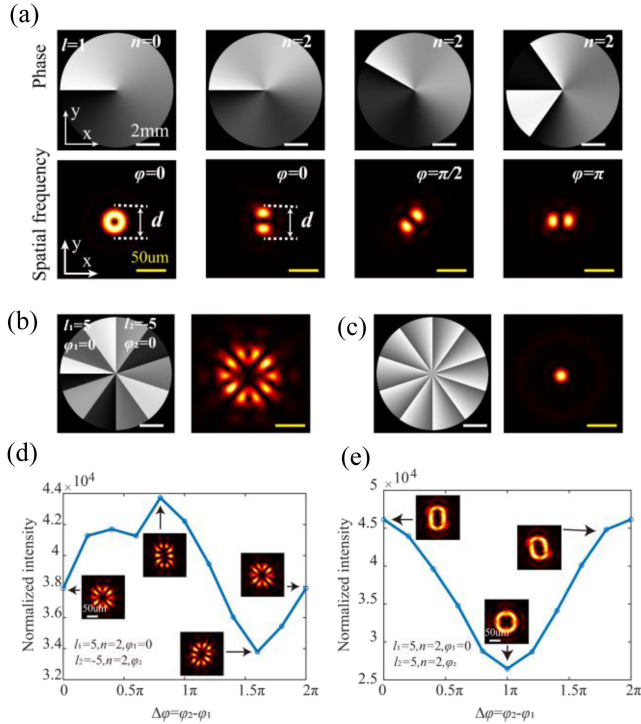
Fig. 1. Selectivity of MOAM holography. (a) MOAM in the frequency domain. (b) MOAM hologram encoded with two image channels $\psi(5, 2, 0)$ and $\psi(-5, 2, 0)$ and reconstruction image. (c) Reconstructed result with mode $\psi(-5, 2, \pi)$. (d) Interaction between two image channels $\psi(5, 2, \varphi_1)$ and $\psi(-5, 2, \varphi_2)$. (e) Interaction between two image channels $\psi(5, 2, \varphi_1)$ and $\psi(5, 2, \varphi_2)$.

Fig. 2. Influencing factors of MOAM holography. (a) Effect of $\Delta\varphi' = \varphi_{de}-\varphi_1$. (b) The ratio of signal intensity and the maximum crosstalk intensity as the function of the multiplexing number. (c) SNR as the function of phase difference $\Delta\varphi$.

beam, which can be expressed as $\psi(l, n, \varphi_i) = \exp[jl\varphi + j\cos(n\varphi + \varphi_i)]$, where j is the imaginary unit, l is the helical phase index, φ is the azimuthal angle, n is the modulating factor used to control the splitting properties of the modulated mode, and φ_i is the phase used to adjust the azimuthal angle [22]. When an incident beam carrying a MOAM is used, the reconstructed electric field at the image plane can be formulated as

$$E_{\text{MOAM}}(x, y) = \boldsymbol{F}[H_{\text{MOAM}}(k_x, k_y)]$$
$$= E(x, y) * \boldsymbol{F}[\psi(l, n, \varphi_i)],$$

where $*$ denotes the convolution operation.

The Fourier transform of a modulated helical mode, which acts as a kernel function in the convolution, is simply reproduced at each pixel of the reconstructed image. In order to avoid spatial overlapping between different image spots, the target image should be sub-sampled. However, different from that of an OAM beam, which is of a doughnut-shaped intensity distribution, the Fourier transform of a MOAM beam obeys a split intensity distribution [Fig. 1(a)]. The number of the split lobes is equal to the modulating factor n, and the anti-clockwisely rotating angle of the split lobes is determined by φ_i/n [24]. By changing the phase φ_i, a series of modulated helical modes can be generated. Then each mode can be encoded into the MOAM hologram.

To demonstrate the selectivity of each MOAM mode in image reconstruction, we design a MOAM hologram by using two dot
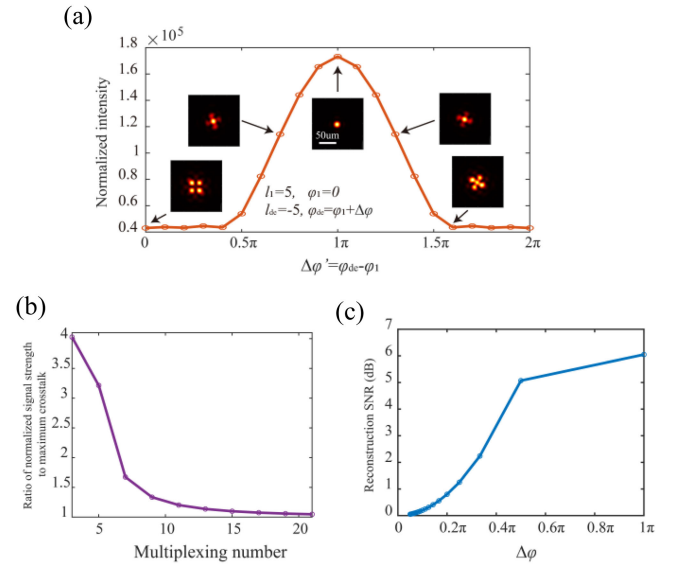
images, which are encoded with the modulating helical phases $\varphi_1 = 0$ and $\varphi_2 = \pi$ [$l = 5$, $n = 2$], respectively [Fig. 1(b)]. When this MOAM hologram is directly illuminated by a planar beam, the reconstructed image has the split intensity [Fig .1(b)]. In the reconstructed image, the interaction between the two image channels is influenced by the difference between the two encoding phases $\Delta\varphi = \varphi_2-\varphi_1$, as shown in Fig. 1(d)–(e). An expected dot-pattern associated with the channel $\psi(l, n, \varphi_i)$ can only be produced when the MOAM hologram is decoded using the corresponding inverse modulated phase mode $\psi(l_{de}, n_{de}, \varphi_{de})$ with $l_{de} = -l$, $n_{de} = n$, and $\varphi_{de} = \pi+\varphi_i$.

The reconstructed peak intensity of the i-th image channel is influenced by the difference between the decoding phase constant and the encoding phase constant $\Delta\varphi' = \varphi_{de}-\varphi_i$ [Fig. 2(a)]. Given a MOAM hologram encoded with $\exp[jl\varphi+j\cos(n\varphi)]$, the resulting beam at the hologram plane can be expressed as $\exp[j\cos(n\varphi)+j\cos(n\varphi+\Delta\varphi')]$ when illuminated by a mismatched mode $\exp[-jl\varphi+j\cos(n\varphi+\Delta\varphi')]$ with $\Delta\varphi'\neq\pi$. Evidently the resulting image will appear as split or doughnut-shaped dots, which have lower peak intensities than that of the expected dot-patterned image channels. Henceforth they are regarded as background disturbance. Suppose a MOAM hologram has M image channels with the same parameters l and n, $E = \sum_{i=1}^{M} \exp[jl\varphi + j\cos(n\varphi + \varphi_i)]$. When it is decoded with $\exp[-jl\varphi+j\cos(n\varphi+\varphi_1+\pi)]$, the desired dot image $\psi(l, n, \varphi_1)$ will become $E_1 = \exp(0) = 1$, implying that it will be converted into a Gaussian spot in the reconstructed image. While the disturbance associated with other channels will cause crosstalk with E_1, $E_{cros} = \sum_{i=2}^{M} \exp[j\cos(n\varphi + \varphi_i)]$. It can be seen from Fig. 2 that the crosstalk between $\psi(l, n, \varphi_1)$ and another channel $\psi(l, n, \varphi_i)$ achieves maximum when $\Delta\varphi_i = \varphi_i-\varphi_1$ is minimum. Therefore, as the multiplexing number M
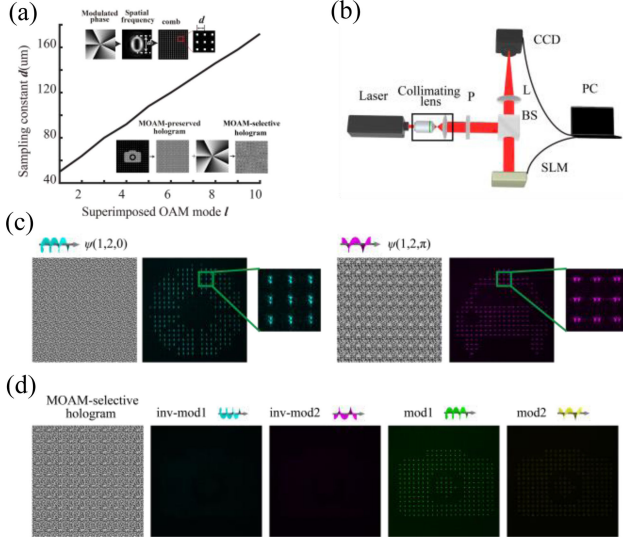
Fig. 3. Experiment of preservation and selectivity of MOAM. (a) The relationship between the sampling constant d and the helical index l. (b) Optical setup. P: linear polarizer; L: lens; BS: beam splitter. (c) Reconstructed images from a planar beam. (d) Reconstruction result.

increases, the disturbance intensity $|F(E_{\text{cro}})|$ will increase gradually, while the signal intensity $|F(E_{\text{sig}})|$ is constant, resulting in a small SNR $= 20\log_{10}[|F(E_{\text{sig}})|/|F(E_{\text{cros}})|]$.

Base on the strong MOAM selectivity, the MOAM hologram can be generated as $E = \sum_{i=1}^{M} A_i e^{j\theta_i} e^{j \arg[\psi(l,n,\varphi_i)]}$. A and θ are the amplitude and phase of each image channel, respectively. θ can be obtained by the Gerchberg-Saxton algorithm [28]. Four modulating phase modes, namely $\psi(5, 2, 0)$, $\psi(5, 2, \pi)$, $\psi(-5, 2, \pi)$ and $\psi(-5, 2, 0)$ are used as an example. For the sake of simplicity, we denote these four modulating modes using 'mod1', 'mod2','inv-mod1' and 'inv-mod2', respectively. The desired image can be reconstructed only when decoded by an appropriate MOAM beam, i.e., each image dot has a fundamental Gaussian distribution.

III. CXPERIMENTAL DEMONSTRATION

A. Preservation and Selectivity of MOAM

The physical mechanism and experimental result of the MOAM holography are shown in Fig. 3. Similar to that in the OAM holography, a hologram should be sampled in its spatial-frequency domain to preserve the MOAM properties, as shown in Fig. 3(a). Usually, the sampling period d is determined by the spatial-frequency bandwidth of the superimposed modulating helical mode. Then a hologram is generated by the Gerchberg-Saxton algorithm [28]. In our experiment, the sampled hologram is not directly illuminated with an incident MOAM beam. Instead, the hologram is equivalently modulated with a helical phase mode and illuminated with a planar wave. To demonstrate the MOAM-preserving property, an experimental system is built as shown in Fig. 3(b). A He-Ne laser with a central wavelength of 632.8 nm is applied as the light source. After being collimated by a lens, polarized by a polarizer, and reflected by
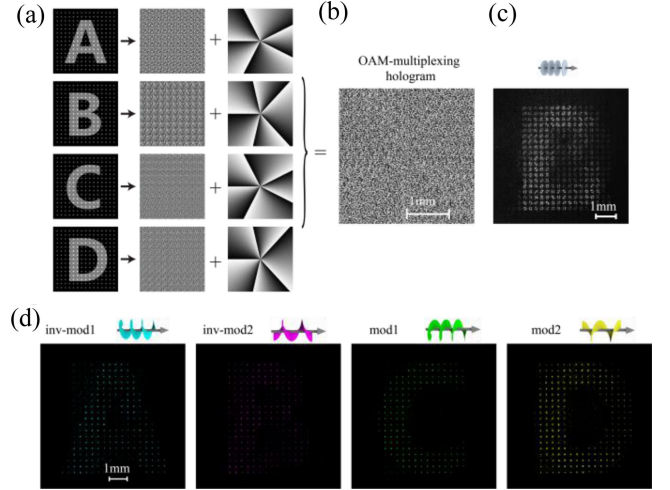

Fig. 4. Experiments of MOAM multiplexation. (a) The design approach. (b) Experimental result. (c) Reconstructed image resulting from a planar wave. (d) Four images resulting from different incident MOAM beams.

a beam splitter, the beam arrives at a spatial light modulator (SLM) Holoeye PLUTO-NIR-011. The SLM has 1080×1920 pixels with a pixel size of 8 μm. Passing through a convex lens with a focal length of 250 mm, the beam arrives at a CCD with 2048×2048 pixels and a pixel size of 5.5 μm. A target image with 400×400 pixels is used, where the sampling period is 10 pixels. Fig. 3(c) shows the experimental results of the reconstructed images. It is clearly seen that each spot in the former image is split into two main lobes [Fig. 3(c)].

The MOAM holography is required to be capable of selecting a particular MOAM mode by using a specially designed illuminating beam. Then different MOAM modes would not be mixed in the reconstructed images, as illustrated in Fig. 3(d). Encoded with a modulating phase map $\psi(5, 2, 0)$, a hologram can be generated [left of Fig. 3(d)], and the experimental results are shown at the right of Fig. 3(d). It is clearly seen that the holographic image shows high quality only when illuminated by a MOAM beam with an inverse modulating helical mode, in which case each pixel in the target is converted into a Gaussian mode with greater intensity.

B. Multi-Image Multiplexation of MOAM

Base on the strong MOAM selectivity, MOAM-multiplexation can be achieved, as illustrated in Fig. 4. As an example, four target images associated with letters "A", "B", "C", and "D" are employed. The four images need to be sampled first to generate MOAM holograms, then the four holograms are encoded with different modulating phase modes 'mod1', 'mod2', 'inv-mod1' and 'inv-mod2', respectively [Fig. 4(a)]. These four phase maps can be superimposed into one MOAM hologram, as shown in Fig. 4(b). As a result, when a planar beam illuminates the hologram, four distinct images can interfere with each other, leading to a complex image pattern [Fig. 4(c)]. However, when the hologram is illuminated separately with different MOAM beams, namely,
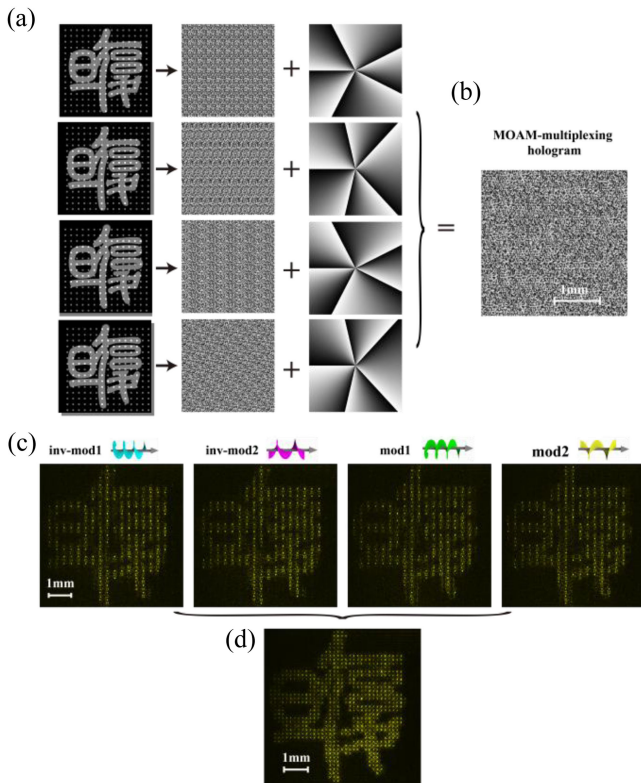
Fig. 5. Experimental results of improving image resolution by MOAM multiplexation. (a) Design approach. (b) Hologram. (c) Reconstruction of four images with different incident MOAM beams. (d) High resolution image by combining four images.

'inv-mod1', 'inv-mod2', 'mod1' and 'mod2', four distinct target images can be individually generated, as shown in Fig. 4(d). Interestingly, the reconstructed image can achieve high quality. The non-uniformity of the reconstructed image in Fig. 4(d) is caused by the crosstalk from other image channels. The experimental results prove that four images can be stored in and extracted from one hologram by using only one helical phase index of an OAM mode. Concerning the crosstalk between different image channels, the peak intensities of the desired letters are about 5 times the disturbance, leading to a SNR of about 7 dB.

C. Resolution Enhancement by MOAM-Multiplexation

In the conventional OAM holography, the image resolution is determined by the sampling period of the target image, which is associated with the helical phase index l. The larger the l, the larger the sampling period of target image. In fact, the image resolution can be improved by MOAM-multiplexation. If regarding a high-resolution image as a combination of several low-resolution images with a lateral shift between each other, the target image can be reconstructed faithfully by processing each low-resolution image individually. As shown in Fig. 5, a target image is composed of four arrays with the same period d. Compared with the first sampling array, the second, third and fourth arrays have shifts $(d/2, 0)$, $(0, -d/2)$ and $(d/2, -d/2)$,

respectively with respect to the first array. The four images can generate four MOAM holograms, and they are encoded with four modulating phase modes 'mod1', 'mod2', 'inv-mod1' and 'inv-mod2', respectively. Then the four phase maps are combined into one MOAM hologram, as shown in Fig. 5(b). It is clearly seen that by using four distinct MOAM beams separately, four low resolution images can in turn be obtained. Interestingly, we can produce a high-resolution image by combining the four low resolution images, as shown in Fig. 5(d), which is about twice the resolution of the OAM holography. As a result, the MOAM holography provides a straightforward way to improving the reconstruction resolution.

IV. SUMMARY

In summary, the modulated orbital angular momentum holography is proposed and experimentally demonstrated. By imposing several cosine-modulated phase modes onto an OAM mode, multiple MOAM modes can be generated. Consequently, the helical phase of an OAM mode can be separated into several modulated phase modes and each can be encoded to a MOAM hologram. In addition, the resolution of the reconstructed images can be improved by multiplexing a helical phase index. Consequently, the MOAM holography proposed in this paper will enhance the holographic information capacity and provide diverse methods for optical encryption and beam manipulations.

REFERENCES

[1] L. Allen, M. W. Beijersbergen, R. J. C. Spreeuw, and J. P. Woerdman, "Orbital angular momentum of light and the transformation of Laguerre-Gaussian laser modes," *Phys. Rev. A*, vol. 45, no. 11, pp. 8185–8189, 1992, doi: 10.1103/PhysRevA.45.8185.

[2] M. Uchida and A. Tonomura, "Generation of electron beams carrying orbital angular momentum," *Nature*, vol. 464, no. 7289, pp. 737–739, 2010, doi: 10.1038/nature08904.

[3] K. Dholakia and T. Čižmár, "Shaping the future of manipulation," *Nat. Photon.*, vol. 5, no. 6, pp. 335–342, 2011, doi: 10.1038/nphoton.2011.80.

[4] M. Padgett and R. Bowman, "Tweezers with a twist," *Nat. Photon.*, vol. 5, no. 6, pp. 343–348, 2011, doi: 10.1038/nphoton.2011.81.

[5] J. Wang *et al.*, "Terabit free-space data transmission employing orbital angular momentum multiplexing," *Nat. Photon.*, vol. 6, no. 7, pp. 488–496, 2012, doi: 10.1038/nphoton.2012.138.

[6] A. E. Willner *et al.*, "Optical communications using orbital angular momentum beams," *Adv. Opt. Photon.*, vol. 7, no. 1, pp. 66–106, 2015, doi: 10.1364/aop.7.000066.

[7] A. M. Yao and M. J. Padgett, "Orbital angular momentum: Origins, behavior and applications," *Adv. Opt. Photon.*, vol. 3, no. 2, pp. 161–204, 2011, doi: 10.1364/aop.3.000161.

[8] H. Ren *et al.*, "Metasurface orbital angular momentum holography," *Nat. Commun.*, vol. 10, no. 1, pp. 1–8, 2019, doi: 10.1038/s41467-019-11030-1.

[9] X. Fang, H. Ren, and M. Gu, "Orbital angular momentum holography for high-security encryption," *Nat. Photon.*, vol. 14, no. 2, pp. 102–108, 2020, doi: 10.1038/s41566-019-0560-x.

[10] H. Ren, X. Fang, J. Jang, J. Bürger, J. Rho, and S. A. Maier, "Complex-amplitude metasurface-based orbital angular momentum holography in momentum space," *Nat. Nanotechnol.*, vol. 15, no. 11, pp. 948–955, 2020, doi: 10.1038/s41565-020-0768-4.

[11] X. Fang *et al.*, "Multiple copies of orbital angular momentum states through second-harmonic generation in a two-dimensional periodically poled litao3 crystal," *Appl. Phys. Lett.*, vol. 107, no. 16, pp. 1–5, 2015, doi: 10.1063/1.4934488.

[12] J. Hamazaki, Y. Mineta, K. Oka, and R. Morita, "Direct observation of gouy phase shift in a propagating optical vortex," *Opt. Exp.*, vol. 14, no. 18, pp. 8382–8392, 2006, doi: 10.1364/oe.14.008382.

[13] A. M. Amaral, E. L. Falcão-Filho, and C. B. de Araújo, "Shaping optical beams with topological charge," *Opt. Lett.*, vol. 38, no. 9, pp. 1579–1581, 2013, doi: 10.1364/ol.38.001579.

[14] N. P. Hermosa and C. O. Manaois, "Phase structure of helico-conical optical beams," *Opt. Commun.*, vol. 271, no. 1, pp. 178–183, 2007, doi: 10.1016/j.optcom.2006.10.004.

[15] C. A. Alonzo, P. J. Rodrigo, and J. Glückstad, "Helico-conical optical beams: A product of helical and conical phase fronts," *Opt. Exp.*, vol. 13, no. 5, pp. 1749–1760, 2005, doi: 10.1364/opex.13.001749.

[16] J. B. Götte *et al.*, "Light beams with fractional orbital angular momentum and their vortex structure," *Opt. Exp.*, vol. 16, no. 2, pp. 993–1006, 2008, doi: 10.1364/oe.16.000993.

[17] A. M. Nugrowati, W. G. Stam, and J. P. Woerdman, "Position measurement of non-integer OAM beams with structurally invariant propagation," *Opt. Exp.*, vol. 20, no. 25, pp. 27429–27441, 2012, doi: 10.1364/oe.20.027429.

[18] Y. Jiang, K. Huang, and X. Lu, "Propagation dynamics of abruptly auto focusing airy beams with optical vortices," *Opt. Exp.*, vol. 20, no. 17, pp. 18579–18584, 2012, doi: 10.1364/oe.20.018579.

[19] T. Ellenbogen, N. Voloch-Bloch, A. Ganany-Padowicz, and A. Arie, "Nonlinear generation and manipulation of airy beams," *Nat. Photon.*, vol. 3, no. 7, pp. 395–398, 2009, doi: 10.1038/nphoton.2009.95.

[20] B. Chen, C. Chen, X. Peng, Y. Peng, M. Zhou, and D. Deng, "Propagation of sharply autofocused ring airy Gaussian vortex beams," *Opt. Exp.*, vol. 23, no. 15, pp. 19288–19298, 2015, doi: 10.1364/OE.23.019288.

[21] X. Chen, D. Deng, G. Wang, X. Yang, and H. Liu, "Abruptly autofocused and rotated circular chirp pearcey Gaussian vortex beams," *Opt. Lett.*, vol. 44, no. 4, pp. 955–958, 2019, doi: 10.1364/ol.44.000955.

[22] X. Chen *et al.*, "Focusing properties of circle pearcey beams," *Opt. Lett.*, vol. 43, no. 15, pp. 3626–3629, 2018, doi: 10.1364/ol.43.003626.

[23] P. Li *et al.*, "Modulation of orbital angular momentum on the propagation dynamics of light fields," *Front. Optoelectron.*, vol. 12, no. 1, pp. 69–87, 2019, doi: 10.1007/s12200-017-0743-3.

[24] F. Wang, C. Lou, and Y. Liang, "Propagation dynamics of ring airy Gaussian beams with cosine modulated optical vortices," *Chin. Opt. Lett.*, vol. 16, no. 11, 2018, Art. no. 110502, doi: 10.3788/col201816.110502.

[25] J. E. Curtis and D. G. Grier, "Modulated optical vortices," *Opt. Lett.*, vol. 28, no. 11, pp. 872–874, 2003, doi: 10.1364/ol.28.000872.

[26] P. Li, S. Liu, T. Peng, G. Xie, X. Gan, and J. Zhao, "Spiral autofocusing airy beams carrying power-exponent-phase vortices," *Opt. Exp.*, vol. 22, no. 7, pp. 7598–7606, 2014, doi: 10.1364/OE.22.007598.

[27] P. Chen *et al.*, "Digitalizing self-assembled chiral superstructures for optical vortex processing," *Adv. Mater.*, vol. 30, no. 10, pp. 1–6, 2018, doi: 10.1002/adma.201705865.

[28] R. W. Gerchberg and W. Saxton, "A practical algorithm for the determination of phase from image and diffraction plane pictures," *Optik*, vol. 35, pp. 237–250, 1971.